The Monoclinic–Orthorhombic Phase Transition in ZSM-5 Zeolite: Spontaneous Strain Variation and Thermodynamic Properties

Matteo Ardit,* Annalisa Martucci, and Giuseppe Cruciani

Physics and Earth Sciences Department, University of Ferrara, via Saragat 1, I-44122 Ferrara, Italy
*corresponding author e-mail: rdtmtt@unife.it

ABSTRACT
Modeling the ferroelastic properties of the monoclinic-orthorhombic phase transition of ZSM-5 zeolites is much relevant to understand the effects of lattice strain on adsorption and diffusion properties of these microporous materials widely used in catalysis and water treatment. Using very accurate synchrotron X-ray diffraction data we report here the analysis of spontaneous strain variation across the transition. According to the Landau theory, the behavior of the order parameter reveals the tricritical character of this transition from ferroelastic to paraelastic phase in ZSM-5. Combination of results from Landau analysis with calorimetric data allows the calculation of thermodynamic quantities which are in good agreement with the experimentally derived ones.

INTRODUCTION

ZSM-5 is a crystalline aluminosilicate zeolite (MFI topology)[1] largely used as solid acid catalysts in several applications due to its high surface area, thermal, mechanical and chemical stability.

The MFI framework type can be described in terms of pentasil chains running parallel to the *c*-axis which are connected via oxygen bridges to form corrugated sheets with 10-ring holes. Adjacent sheets are related to one another by an inversion center thus producing straight 10-ring channels parallel to the corrugations (along *b*), and sinusoidal 10-ring channels perpendicular to the sheets (along *a*).[1] Sinusoidal and straight channels are linked to one another to form a 3-dimensional 10-ring channel system. The MFI topological symmetry is orthorhombic *Pnma*, which is observed in as-synthesized ZSM-5.

From the crystallographic point of view all synthetic MFI zeolites exhibit a polymorphic monoclinic ($P2_1/n$) -to- orthorhombic (*Pnma, Pn*2_1a or $P\ 2_12_12_1$) phase transition with varying composition,[2-11] framework defect density,[12] temperature,[3,13-17] or nature and amount of guest compounds in the channels systems.[18-28]

In as-synthesized ZSM-5 obtained in alkaline medium and in the presence of tetrapropylammonium (TPA) template molecule, the crystal symmetry is orthorhombic, space group *Pnma,* with 12 independent T-sites in the unit cell. After template removal by calcination the ZSM-5 orthorhombic structure undergoes a monoclinic symmetry change (space group $P2_1/n$) with 24 independent T-atoms in the unit cell. Monoclinic MFI crystals consists of an aggregate of monoclinic twin domains which exhibit a reversible phase transition to a single-crystal orthorhombic phase after adsorption of bulky aromatic compounds other than benzene.[3,21,22,27] Reported for the first time by Wu et al. in 1979,[14] such a reversible phase transition is described as a mutual shift of successive (010) pentasil layers along the *c*-axis, associated to a small change in the Si–O–Si bond angles and Si–O bond distances.[3,6] However, after adsorption of benzene or small sorbate molecules the crystal system is maintained monoclinic.[21,29-31] Twin MFI crystals also trigger a transition into the orthorhombic phase at about 340 K.[6,7] The transition temperature (T_c) can vary in a broad *T*-range (i.e. between 320 and 370 K), depending on the Si/Al ratio, increasing Al content decreases T_c.[13] Furthermore, it was demonstrated that the monoclinic polymorph has the features of a ferroelastic material:[13] the population of the twin domains changes by applying an appropriate mechanical stress.[3,16]

Although some works deal with the thermodynamic of the monoclinic to orthorhombic ($m\leftrightarrow o$) ZSM-5 phase transition,[13,18,32] an investigation centered on the lattice evolution associated to the ferroelastic behavior and the thermodynamic processes within such a phase transition is lacking.

In this contribution, *in situ* high-temperature synchrotron X-ray powder diffraction data have been used to determine the lattice parameter variations of highly siliceous ZSM-5 zeolite across the $m\leftrightarrow o$ phase transition, in the temperature interval 308–573 K.

EXPERIMENTAL SECTION

Sample description. The ZSM-5 sample used in this work was a hydrophobic zeolite (code CBV 28014) provided by Zeolyst International in its ammonium form and used as received. The manufacturer of the CBV 28014 zeolite reports a SiO_2/Al_2O_3 molar ratio equal to 280, a Na_2O content lower than 0.05 wt.% and a surface area of 400 $m^2\ g^{-1}$.

XRPD at high-temperature: data collection and cell refinement strategy. *In situ* high-temperature X-ray diffraction experiments were conducted at the high-resolution powder diffraction beamline ID31 at the European Synchrotron Radiation Facility, ESRF (Grenoble, France). Once diffracted, the incident X-ray (λ = 0.400031 Å) was directed through nine Si 111 analyser crystals and then collected in parallel by means of nine detectors. A subsequent data-reduction was performed to produce the equivalent step scan. X-ray diffraction patterns were recorded every 5 K from 308 to 573 K in air with a heating rate of 0.083 K s^{-1}, in the 0.5–19.5 2θ range.

Figure 1 shows the evolution of the investigated ZSM-5 sample close to the expected transition temperature, T_c, in the 3.80–4.08 (Fig. 1A) and 6.07–6.35 (Fig. 1B) degrees of 2θ.

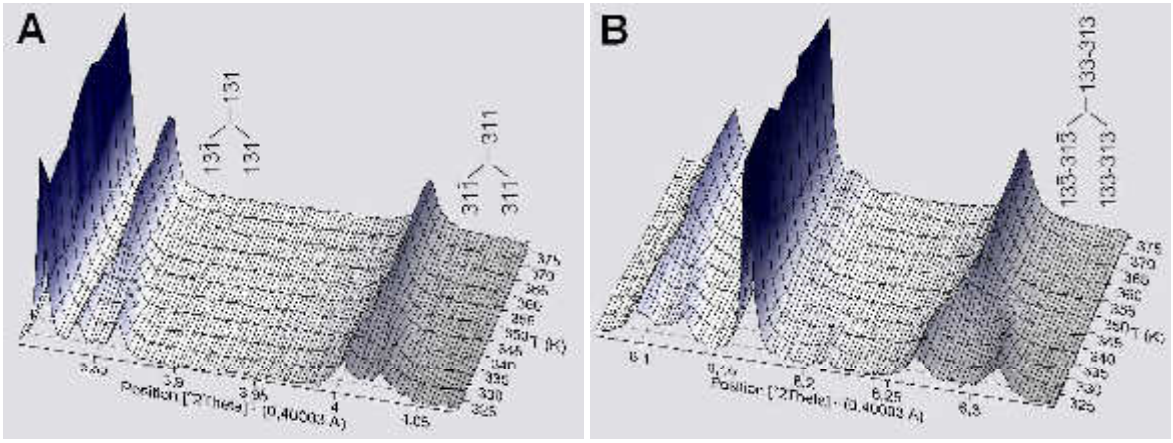

Figure 1. Cascade plot of ZSM-5 sample in the 3.80–4.08 (A) and 6.07–6.35 (B) °2θ ranges within the 321–376 K temperature interval.

An automatic indexing of the peaks, performed by means of the HighScore Plus v.3.0 software in the previously identified angular ranges, revealed that several doublets of peaks gradually move to a single one. In detail, the gradual overlapping of four groups of peaks (i.e. 131 + 13-1 and 311 + 31-1 in the first angular range, and 133 + 13-3 and 313 + 31-3 in the second range) reveals the potential second-order nature of the monoclinic to orthorhombic phase transition, with a T_c close to 350 ± 5 K.

EXPGUI v.1208 interface,[33] for GSAS program,[34] was used to achieve the ZSM-5 cell parameters. Monoclinic and orthorhombic refinements were performed starting from the atomic models of Pasti et al.,[20] and van Koningsveld et al.,[35] respectively. The choice of the space groups (i.e. $P12_1/n1$ for the monoclinic and *Pmnb* for the orthorhombic structures), with a different setting compared to those from literature (i.e. $P2_1/n11$ and *Pnma*, respectively), allow a continuous variation of lattice parameters from the monoclinic to the orthorhombic polymorphs (see "Lattice parameter evolution" in the "Results and discussion" section).

Thermal analysis. Thermogravimetric (TG) and differential thermal analysis (DTA) measurements of the ZSM-5 sample were performed in air at up to 1173 K using a Netzsch STA 409 PC LUXX® - simultaneous TG/DTA thermogravimetric analyzer operating at 10 °C/min heating rate. The thermal curves are reported in Figure 2.

Differential scanning calorimetry. Calorimetric analysis were performed by means of a differential calorimeter (TA instruments, model DSC Q2000) previously calibrated with both pure α-Al_2O_3 and In as standards. 15 mg of the ZSM-5 sample were placed in a unsealed aluminum crucible and underwent 3 cycles of heating and subsequent cooling from 243 to 673 K, with a thermal rate of 0.167 K s^{-1}.

The iterative process of heating and cooling allowed the complete dehydration of the sample. Hence, the enthalpy change achieved from DSC measurements was that exclusively due to the monoclinic to orthorhombic phase transition of the ZSM-5 structure.

Table 1. High-temperature lattice parameters, components of the spontaneous strain tensor ($e_i \times 10^{-3}$), scalar spontaneous strain ($\varepsilon_{ss} \times 10^{-3}$), and volume strain ($V_s \times 10^{-3}$). Figures in parentheses represent one standard-deviation error.

T(K)	a(Å)	b(Å)	c(Å)	β(°)	V(Å^3)	e_{11}	e_{22}	e_{33}	e_{13}	ε_{ss}	V_s
308	19.9079(2)	20.1332(2)	13.3929(2)	90.544(1)	5367.77(15)	-0.99	0.57	-0.96	-4.74	9.60	-1.39
311	19.9096(2)	20.1336(2)	13.3943(2)	90.524(1)	5368.92(15)	-0.93	0.58	-0.87	-4.57	9.24	-1.23
317	19.9117(2)	20.1337(2)	13.3956(2)	90.497(1)	5370.05(15)	-0.88	0.57	-0.80	-4.33	8.77	-1.12
321	19.9136(2)	20.1335(2)	13.3970(2)	90.473(1)	5371.09(15)	-0.81	0.55	-0.71	-4.12	8.34	-0.98
327	19.9170(3)	20.1335(3)	13.3989(2)	90.438(1)	5372.76(15)	-0.69	0.54	-0.59	-3.82	7.71	-0.76
333	19.9197(3)	20.1325(3)	13.4007(2)	90.393(1)	5374.02(16)	-0.60	0.48	-0.47	-3.43	6.92	-0.60
338	19.9234(3)	20.1306(3)	13.4033(2)	90.319(1)	5375.57(16)	-0.45	0.38	-0.29	-2.78	5.60	-0.37
343	19.9312(3)	20.1265(3)	13.4058(2)	90.171(1)	5377.67(17)	-0.09	0.17	-0.11	-1.49	2.99	-0.04
349	19.9331(3)	20.1245(2)	13.4071(2)	90.103(1)	5378.17(15)	-0.03	0.07	-0.02	-0.90	1.80	0.00
349	19.9334(3)	20.1240(3)	13.4074(2)	90.0	5378.23(17)	-0.02	0.04	0.00	0.00	0.05	0.01
354	19.9347(2)	20.1235(2)	13.4077(2)	90.0	5378.56(15)	0.02	0.02	0.01	0.00	0.02	0.03
360	19.9350(2)	20.1232(2)	13.4077(2)	90.0	5378.62(14)	0.01	0.00	0.00	0.00	0.01	-0.01
365	19.9357(2)	20.1235(2)	13.4081(2)	90.0	5379.01(13)	0.01	0.01	0.02	0.00	0.03	0.03
370	19.9359(2)	20.1233(2)	13.4082(2)	90.0	5379.05(13)	0.00	0.00	0.02	0.00	0.02	0.01
376	19.9365(2)	20.1230(2)	13.4082(2)	90.0	5379.12(13)	0.01	-0.01	0.01	0.00	0.02	0.00
381	19.9370(2)	20.1233(2)	13.4082(2)	90.0	5379.35(13)	0.02	0.01	0.01	0.00	0.02	0.02
387	19.9370(2)	20.1230(2)	13.4083(2)	90.0	5379.31(13)	0.00	0.00	0.01	0.00	0.01	-0.01
391	19.9373(2)	20.1231(2)	13.4083(2)	90.0	5379.45(13)	0.00	0.01	0.01	0.00	0.02	0.01
397	19.9376(2)	20.1228(2)	13.4081(2)	90.0	5379.33(12)	0.00	0.00	-0.01	0.00	0.01	-0.02
402	19.9380(2)	20.1231(2)	13.4082(2)	90.0	5379.56(12)	0.01	0.02	0.00	0.00	0.02	0.02
408	19.9379(2)	20.1227(2)	13.4080(2)	90.0	5379.35(12)	-0.01	0.01	-0.01	0.00	0.01	-0.02
413	19.9379(2)	20.1225(2)	13.4082(2)	90.0	5379.37(12)	-0.02	0.01	0.01	0.00	0.02	-0.01
419	19.9378(2)	20.1221(2)	13.4081(2)	90.0	5379.19(12)	-0.03	0.00	0.00	0.00	0.03	-0.04
425	19.9382(2)	20.1222(2)	13.4078(2)	90.0	5379.22(12)	-0.02	0.02	-0.01	0.00	0.03	-0.02
430	19.9385(2)	20.1216(2)	13.4078(2)	90.0	5379.17(13)	-0.01	0.00	0.00	0.00	0.01	-0.01
436	19.9385(2)	20.1217(2)	13.4075(2)	90.0	5379.01(12)	-0.01	0.02	-0.02	0.00	0.03	-0.02
441	19.9383(2)	20.1210(2)	13.4076(2)	90.0	5378.82(12)	-0.02	-0.01	-0.01	0.00	0.02	-0.04
447	19.9382(2)	20.1206(2)	13.4073(2)	90.0	5378.59(12)	-0.03	-0.01	-0.02	0.00	0.03	-0.05
452	19.9388(2)	20.1206(2)	13.4072(2)	90.0	5378.71(12)	0.00	0.01	-0.01	0.00	0.01	-0.01
457	19.9389(2)	20.1201(2)	13.4071(2)	90.0	5378.55(12)	0.01	0.00	-0.01	0.00	0.01	-0.01
463	19.9384(2)	20.1200(2)	13.4071(2)	90.0	5378.39(12)	-0.01	0.01	0.00	0.00	0.02	0.00
468	19.9385(2)	20.1195(2)	13.4070(2)	90.0	5378.26(12)	0.00	0.01	0.00	0.00	0.01	0.01
473	19.9385(2)	20.1192(2)	13.4068(2)	90.0	5378.10(12)	0.00	0.00	0.00	0.00	0.00	0.01
479	19.9385(2)	20.1186(2)	13.4067(2)	90.0	5377.87(12)	0.00	0.00	0.01	0.00	0.01	0.01
484	19.9386(2)	20.1184(2)	13.4068(2)	90.0	5377.91(12)	0.01	0.00	0.03	0.00	0.03	0.05
490	19.9383(2)	20.1177(2)	13.4062(2)	90.0	5377.41(12)	0.01	-0.01	0.00	0.00	0.01	0.00
495	19.9383(2)	20.1175(2)	13.4063(2)	90.0	5377.39(12)	0.01	0.01	0.02	0.00	0.02	0.04
501	19.9386(2)	20.1174(2)	13.4062(2)	90.0	5377.42(12)	0.04	0.03	0.03	0.00	0.05	0.09
506	19.9382(2)	20.1168(2)	13.4060(2)	90.0	5377.02(12)	0.02	0.01	0.02	0.00	0.03	0.06
512	19.9381(2)	20.1161(2)	13.4059(2)	90.0	5376.79(12)	0.02	0.01	0.03	0.00	0.04	0.07
517	19.9379(2)	20.1157(2)	13.4056(2)	90.0	5376.51(12)	0.02	0.01	0.02	0.00	0.03	0.06
523	19.9375(2)	20.1149(2)	13.4053(1)	90.0	5376.07(11)	0.01	0.00	0.01	0.00	0.02	0.03
528	19.9367(2)	20.1138(2)	13.4047(1)	90.0	5375.31(10)	-0.02	-0.04	-0.02	0.00	0.04	-0.07
533	19.9364(2)	20.1134(2)	13.4045(1)	90.0	5375.02(10)	-0.03	-0.03	-0.02	0.00	0.05	-0.08
538	19.9359(2)	20.1128(2)	13.4043(1)	90.0	5374.69(10)	-0.04	-0.03	-0.02	0.00	0.06	-0.10
544	19.9363(2)	20.1125(2)	13.4043(1)	90.0	5374.70(10)	-0.01	-0.02	-0.01	0.00	0.03	-0.04
549	19.9359(2)	20.1121(2)	13.4039(1)	90.0	5374.32(11)	-0.03	-0.02	-0.02	0.00	0.04	-0.07
555	19.9359(2)	20.1116(2)	13.4037(1)	90.0	5374.13(11)	-0.02	-0.01	-0.02	0.00	0.03	-0.05
561	19.9359(2)	20.1116(2)	13.4037(1)	90.0	5374.12(11)	-0.01	0.02	-0.01	0.00	0.02	0.00
566	19.9361(2)	20.1110(2)	13.4036(1)	90.0	5373.99(11)	0.01	0.01	-0.01	0.00	0.02	0.02
571	19.9360(2)	20.1106(2)	13.4038(1)	90.0	5373.92(11)	0.01	0.02	0.01	0.00	0.03	0.04
572	19.9359(2)	20.1106(2)	13.4036(1)	90.0	5373.83(11)	0.01	0.03	0.00	0.00	0.03	0.03
573	19.9354(2)	20.1102(2)	13.4036(1)	90.0	5373.58(11)	-0.01	0.01	0.00	0.00	0.02	0.00

RESULTS and DISCUSSION

Interpretation of the thermal analyses. Thermogravimetric analysis (TG) of ZSM-5 revealed that the total weight loss at 1173 K is about 3.5 %. In particular, the TG curve shows a sudden change in its slope between 295–420 K, which is associated to a ~2.5 % loss in weight. In the same

temperature range, DTA (T_{peak} ~368 K) and DTG (T_{peak} ~368 K) curves show an endothermic event which can be ascribed to both the desorption of water molecules weakly bonded to the surface and to the phase transition, the latter effect being relatively weak compared to the former. The weight loss (~0.45 %) occurring at higher temperatures (i.e. ~420–615 K temperature range) can be ascribed to water molecules hosted in the ZSM-5 channel system. The further weight loss (~0.5 %) at temperatures higher than 615K is strictly related to the decomposition and expulsion of residual NH_4 molecules (DTA T_{peak} ~680K).

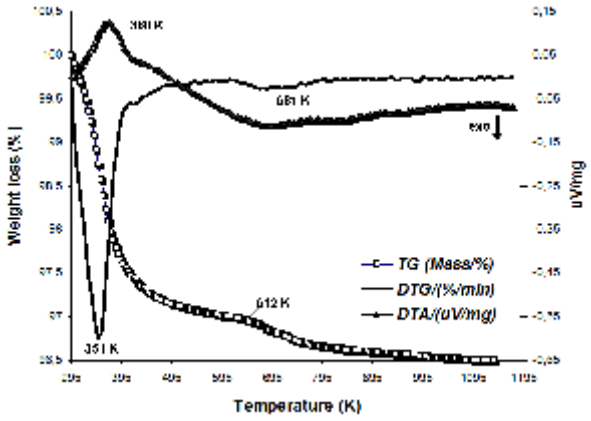

Figure 2. The simultaneous thermogravimetry (TG) - differential thermogravimetry (DTG) - differential thermal analyses (DTA) of ZSM-5 in the temperature range 295–1173 K.

Lattice parameter evolution. The complete set of lattice parameters is given in Table 1 and illustrated as a function of temperature in Figure 3.

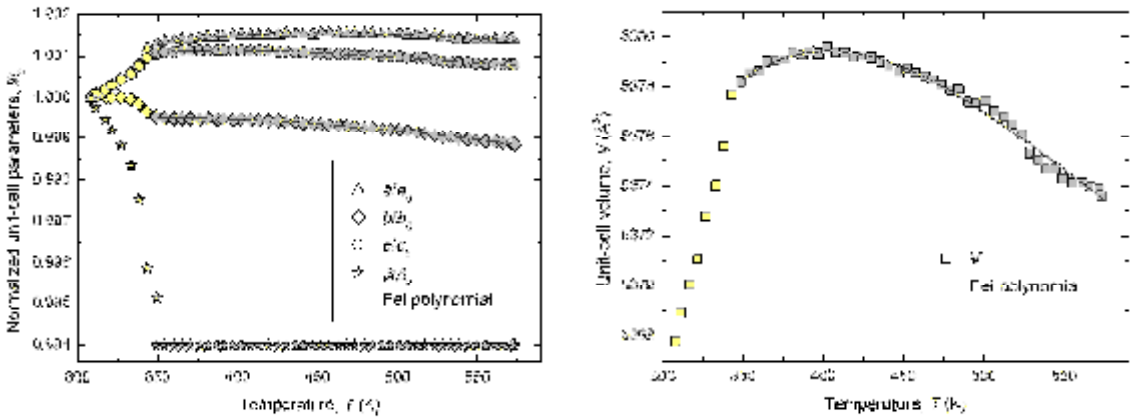

Figure 3. Temperature dependence of lattice parameters (normalized unit-cell edges and β angle, and unit-cell volume, respectively) obtained during a heating cycle from 308 to 573 K. Yellow filled symbols refer to lattice parameters of the $P2_1/n$ monoclinic structure, whereas gray filled symbols are those of the *Pmnb* orthorhombic structure after the phase transition. Standard-deviation errors are within the symbol size. Solid lines through gray symbols are those fitted to the polynomial equation 1.

Although the refined lattice parameters vary continuously on increasing temperature, a strong change in their evolution is detected approaching the transition temperature, i.e. at about T_c = 350 K. In particular, up to this temperature *a* and *c* cell-axes have the same rate of expansion while, in an antithetic manner, the *b*-axis undergoes a contraction. At temperatures higher than that of transition, unit-cell parameters vary more gradually. As a common feature, unit-cell axes show constant values (*b*- and *c*-axis) or a very small increase (*a*-axis) up to about 400 K; thereafter, lattice

parameters show a slight but constant decrease until the maximum temperature investigated is reached. The variations of above are reflected in the evolution of the unit-cell volume, *V*. Indeed, on increasing temperature, a strong volume expansion is detected up to about 350 K (δV = 10.40 Å^3). In the 350–400 K temperature range, the rate of expansion is drastically reduced (10 times lower) until the zeolite structure reach its maximum volume (i.e. up to 5379.56 Å^3 with a δV = 1.39 Å^3). Above 400 K the structure undergoes a continuous negative expansion with a volume reduction of 5.98 Å^3.

Strain analysis. Since the spontaneous strain is an excess property, the components of the spontaneous strain tensor have to be calculated by extrapolating the lattice parameters of the high-symmetry phase (i.e. the paraelastic phase) into the temperature regime of the low-symmetry phase (i.e. the ferroelastic phase) by means of a thermal expansion model.[36,37]
Given that the $m \leftrightarrow o$ phase transition in the ZSM-5 structure takes place at temperatures far from a possible saturation of thermal expansion, which usually occurs at low temperature,[38] the temperature evolution of the *Pmnb* paraelastic phase can be properly described using a polynomial expression (as implemented in EosFit7c)[39] of the form:

$$\alpha = \alpha_0 + \alpha_1 T + \alpha_2 T^{-2} \quad (1)$$

where the mean thermal expansion coefficient α is expressed in K^{-1}, while constants from fits to the experimental data α_0, α_1, and α_2, are expressed in K^{-1}, K^{-2}, and K, respectively.[40] Values of the constants derived by applying Equation 1 to lattice parameters of the *Pnmb* structure are reported in Table 2. Furthermore, resulting fits of Equation 1 to lattice parameters at temperature higher than 349 K are visualized as solid curves in Figure 3.

Table 2. Values of constants in equation 1 (with $\alpha_0 \times 10^{-5}$, $\alpha_1 \times 10^{-8}$, and α_2 in K^{-1}, K^{-2}, and K, respectively) obtained from fits to lattice parameters of the *Pnmb* orthorhombic ZSM-5 structure. $\alpha_{(350\text{-}580)}$ ($\times 10^{-6}$ in K^{-1}) is the mean thermal expansion coefficient calculated in the 340–580 K temperature interval.

	a		*b*		*c*		*V*	
	a_0 = 19.925(1)	α_0 = –2.4(8) α_1 = 2.5(11) α_2 = 2.6(5)	b_0 = 20.120(1)	α_0 = –1.8(7) α_1 = 1.3(10) α_2 = 1.8(5)	c_0 = 13.404(1)	α_0 = –2.7(7) α_1 = 3.0(9) α_2 = 2.3(5)	V_0 = 5373.4(8)	α_0 = –6.8(19) α_1 = 7(3) α_2 = 6.6(13)
$\alpha_{(350\text{–}580)}$	0.31		–2.96		–1.40		–4.03	

When calculated in the same temperature interval (i.e. from 423 to 873 K), the mean volumetric thermal expansion coefficient of the ZSM-5 structure is very close to that reported for a sample of silicalite (a silica polymorph of ZSM-5);[41] specifically $\alpha_{V(423\text{–}873)}$ are –6.43 × 10^{-6} and –7.60 × 10^{-6} K^{-1} for the orthorhombic ZSM-5 and silicalite, respectively.
According to Carpenter et al.,[37] the components of the spontaneous strain tensor for a monoclinic–orthorhombic phase transition are given by:

$$e_{11} = a/a_0 - 1 \quad (2)$$

$$e_{22} = b/b_0 - 1 \quad (3)$$

$$e_{33} = (c/c_0 \sin\beta) - 1 \quad (4)$$

$$e_{13} = 1/2\ (c/c_0 \cos\beta) \quad (5)$$

$$e_{12} = e_{23} = 0 \quad (6)$$

where a_0, b_0, and c_0 are lattice parameters of the *Pmnb* structure extrapolated into the stability field of the $P2_1/n$ ferroelastic structure.
In an analogous way the volume strain, V_s, is given by:

$$V_s = V/V_0 - 1 \quad (7)$$

Furthermore, as measure of the total strain due to the $m \leftrightarrow o$ phase transition,[36,37] the scalar spontaneous strain, ε_{ss}, has been calculated as:

$$\varepsilon_{ss} = (e_{11}^2 + e_{22}^2 + e_{33}^2 + 2e_{13}^2)^{1/2} \quad (8)$$

Strains e_i, ε_{ss}, and V_s, calculated from lattice parameters by means of the above equations are listed in Table 1. Their variation is visualized as a function of temperature in Figure 4.

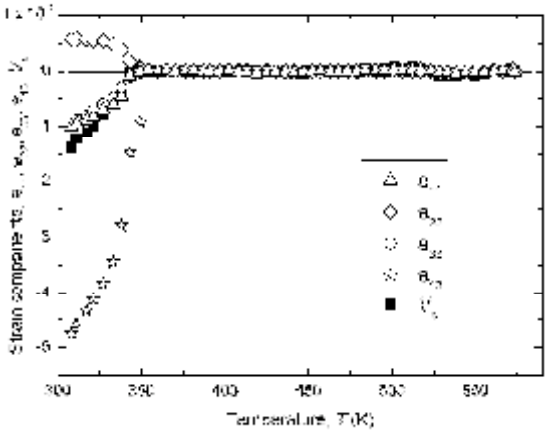

Figure 4. Temperature evolution of spontaneous strain components and volume strain due to the $m \leftrightarrow o$ phase transition in ZSM-5 structure (cfr. Equations 2–7).

Order parameter and character of the phase transition. As stated in the introduction, the $m \leftrightarrow o$ phase transition occurring in the ZSM-5 zeolite structure is reversible with displacive features.[14] Firstly ascribed to a mutual shift of successive (100) pentasil layers along *c*,[6] the symmetry change in the ZSM-5 upon heating was later described as a complex displacement of the framework atoms, which mostly affects Si–O–Si angles within the 10-membered tetrahedral rings.[4] The latter authors also highlighted that the monoclinic polymorph of the ZSM-5 structure has the features of a ferroelastic material,[3] which belongs to the "Aizu-type" *mmm***F**2/*m*.[42]
The present strain analyses revealed that, when the point group *mmm* (orthorhombic) changes into 2/*m* (monoclinic), the primary order parameter, Q, behaves as the symmetry-adapted strain. This means that a proper spontaneous strain is involved, and the order parameter can be coupled with the largest component of the spontaneous strain, e_{13}.[36,42] This shear strain is determined, as reported in the previous section, from the variation of the monoclinic β angle.
In order to validate the symmetry criteria by which the strain components and the primary order parameter are coupled, some tests for internal consistency of the strain variation are applied. In the specific case of the $m \leftrightarrow o$ phase transition in the ZSM-5 structure, it is expected that: 1) the variation of the volume strain (V_s) is equivalent to the sum of the strain tensor components parallel to the three reference axes (i.e. $e_{11} + e_{22} + e_{33}$) [Figure 5A]; 2) the primary order parameter and the scalar spontaneous strain, which have the same symmetry, are proportional (i.e. $Q \propto \varepsilon_{ss}$) [Figure 5B]; 3) the volume strain (V_s) varies linearly with Q^2 [Figure 5C].[37]
Strain/strain plots in Figure 5 clearly show that all of above considerations are verified.

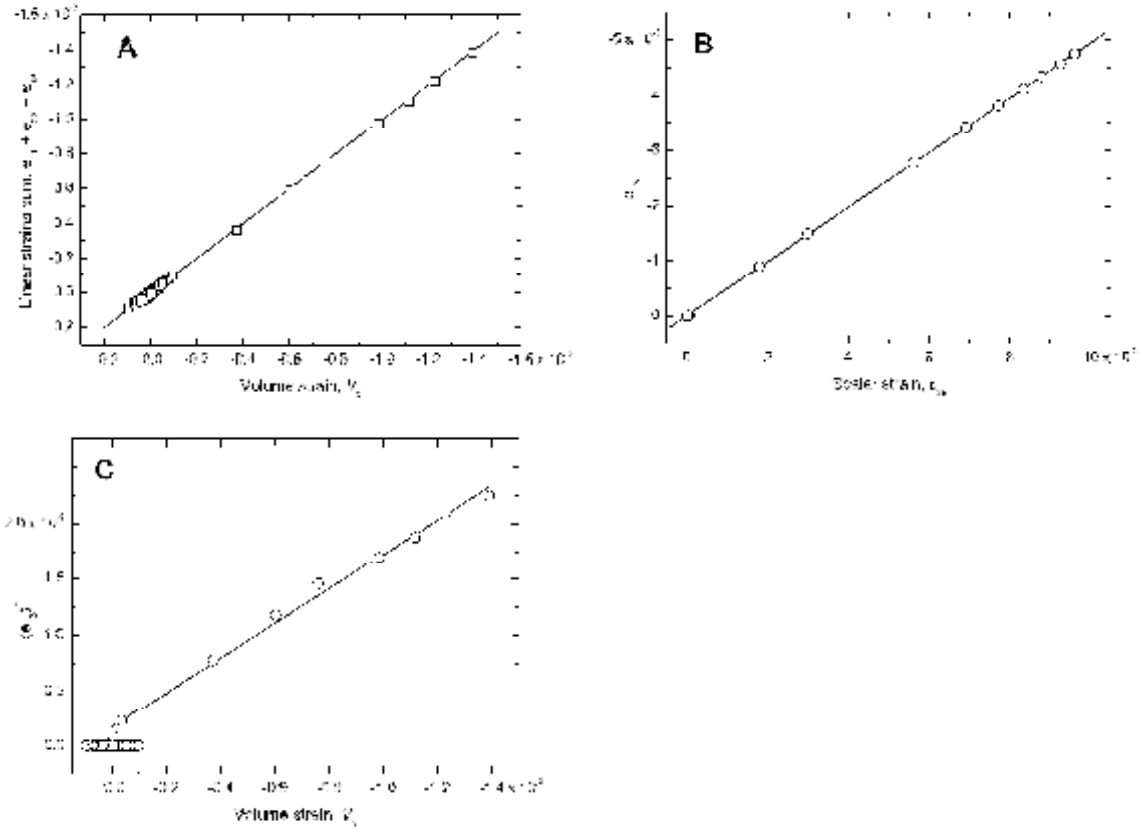

Figure 5. Strain/strain plots for the $P2_1/n \leftrightarrow Pmnb$ phase transition in the ZSM-5 structure upon heating. Sum of the linear strains e_{11}, e_{22}, and e_{33} as a function of the volume strain V_s variation (A); shear strain component e_{13} (regarded as the primary order parameter) as a function of the scalar spontaneous strain ε_{ss} (B); and volume strain V_s dependence of the square of the shear strain component e_{13} (C). See text for further details.

Hence, on the base of the Landau theory, it is now possible to describe the excess thermodynamic quantities due to the ZSM-5 $m \leftrightarrow o$ phase transition through a polynomial expansion (a 246 Landau potential) of the order parameter Q, having the form:[36,37,43]

$$G(Q) = A/2(T-T_c)Q^2 + B/4Q^4 + C/6Q^6 \quad (9)$$

where a, b, and c are Landau coefficients and Q is the order parameter of the phase transition.
From the previous Equation 9, the transition temperature T_c, as well as the ratios of the Landau coefficients, can be derived by fitting the temperature dependence of the primary ferroelastic order parameter into the equation which follows:[37,43,44]

$$T = T_c - B/AQ^2 - C/AQ^4 \quad (10)$$

Figure 6 shows the variation of the shear strain component e_{13} with temperature. Its evolution is perfectly described by Equation 10 (solid line in Figure 6) for Landau coefficients ratios equal to $B/A = 8.3(3) \times 10^5$ K and $C/A = 4.2(1.1) \times 10^{10}$ K, with a fitted transition temperature $T_c = 348(1)$ K.

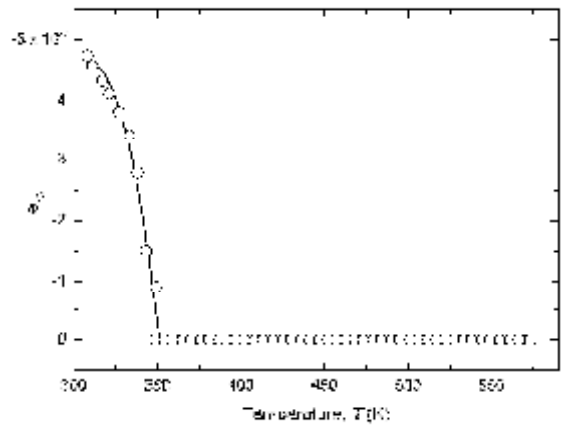

Figure 6. Temperature dependence of the spontaneous strain tensor component e_{13}, which behaves as the primary order parameter Q for the $P2_1/n \leftrightarrow Pmnb$ phase transition. Solid line represents the fit of Equation 9 to the calculated e_{13} from lattice parameters.

An inspection on the ratios of the Landau coefficients reveals that $C/A \gg B/A$. This means that the ZSM-5 $m \leftrightarrow o$ phase transition occurring at T_c = 348(1) K is close to the critical point.[44]

As shown in Figure 6, the temperature dependence of the shear strain component e_{13}, which behaves as the primary order parameter Q for the $P2_1/n \leftrightarrow Pmnb$ phase transition, is continuous (i.e. the Q evolution presents no jumps, meaning that the first derivative of the free energy $\partial G/\partial T$ is continuous). Hence, the temperature dependence of Q up to $T = T_c$ should follow the relationship:[43]

$$Q = |(T_c - T)/T_c|^{\beta} \qquad \text{with } ¼ \leq \beta \leq ½ \qquad (11)$$

Since such a phase transition is recognized to be close to the critical point, the exponent $\beta \rightarrow ¼$.[36,43] Figure 7 unequivocally shows that, upon heating, the ZSM-5 structure undergoes a phase transition which can be ascribed as tricritical, within experimental uncertainty.

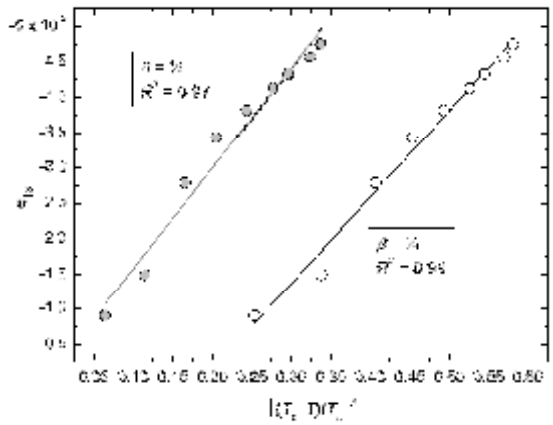

Figure 7. Appraisal of the tricritical phase transition in ZSM-5 zeolite upon heating.

Calorimetric analysis. Figure 8 shows experimental DSC curves for the studied ZSM-5 sample on heating (A) and cooling (B) in the temperature range affected by the $m \leftrightarrow o$ phase transition, i.e. close to T_c = 348(1) K. The $m \leftrightarrow o$ phase transition is observed to extend in a quite large temperature interval, ΔT = 56 K on heating, with a maximum endothermic peak located at about 340 K (Figure 8A). Furthermore, a comparison between Figure 8A and 8B reveals that a same amount of enthalpy

change is involved in both heating and cooling processes. A deconvolution of these peaks leads to an averaged enthalpy change $\Delta H = 2.8$ kJ·mol^{-1}.
All these features suggest that the ZSM-5 *m*↔*o* phase transition is subtle, reversible and they confirm its displacive nature.[14]

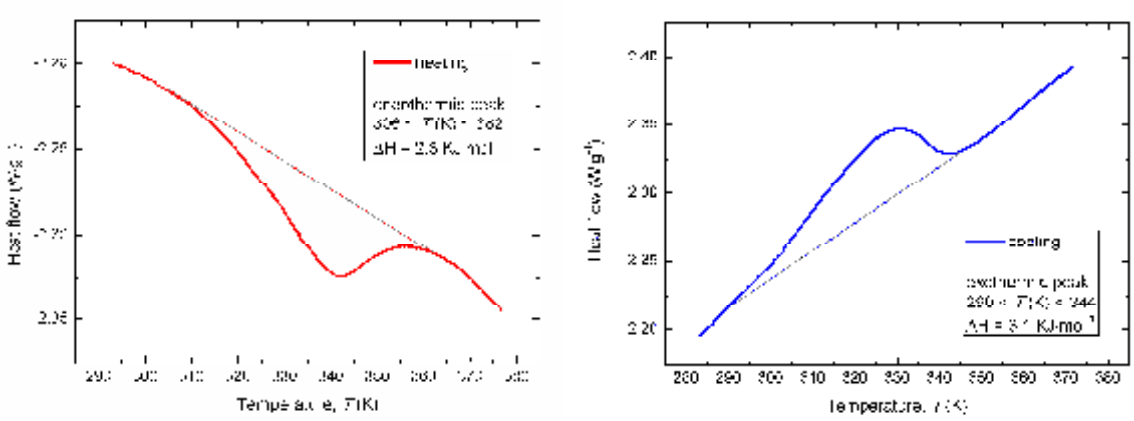

Figure 8. Heating (on the left) and cooling (on the right) DSC curves near the transition temperature, T_c = 348(1) K. Heating and cooling rate: 0.167 K s^{-1}.

In Figure 9, the variation of enthalpy associated to the reversible *m*↔*o* phase transition in several MFI zeolites is plotted as a function of the aluminum content for each zeolitic framework. As well schematized in this figure, our results are in agreement with those previously observed in other studies for compounds having a similar Si/Al ratio. Once plotted with the same molar unit (i.e. a mole of anhydrous MFI zeolite weighted for the Al content), all data in Figure 9 define, albeit with a modest degree of scatter, a curve with an exponential trend subordinated to the aluminum content.

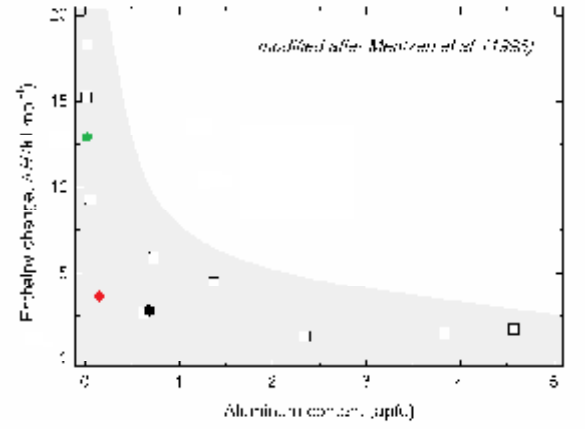

Figure 9. Enthalpy change associated to the reversible *m*↔*o* phase transition in anhydrous MFI samples as a function of the aluminum content of the zeolitic framework (modified after Mentzen et al., 1996).[13] Symbol map: white squares (Mentzen et al. 1996; and references therein);[13] black hexagon (*this work*); red diamond (Endoh 1988);[17] green circle (Boerio-Goates et al. 2002; value multiplied by 96 because the published datum refers to a mole of SiO_2).[32]

Deriving other excess thermodynamic properties. Once nature of the phase transition and the associated enthalpy change are known it is possible to derive other excess thermodynamic properties (e.g. the excess entropy for *m*↔*o* phase transition). Assuming the nature of the ZSM-5 phase transition as purely tricritical (i.e. the *B* coefficient is negligible) the excess free energy expression of Equation 9 can be simplified as:

$$G(Q) = A/2(T-T_c)Q^2 + C/6Q^6 \quad (12)$$

Consequently, the equilibrium variation of Q with T is:

$$Q = A/C(T-Tc)^{1/4} \qquad \text{with } Tc = C/A \quad (13)$$

By this way, the excess enthalpy as well as the excess entropy of the phase transition can be calculated by means:[43]

$$\Delta H = -A/2TcQ^2 + C/6Q^6 \quad (14)$$

and

$$\Delta S = -A/2Q^2 \quad (15)$$

As previously reported, the total excess enthalpy associated to the $m \leftrightarrow o$ phase transition in the ZSM-5 structure with increasing temperature is found to be ΔH = 2.8 kJ·mol^{-1}. Substituting this value into the Equation 14, A and C Landau coefficients can be readily calculated (i.e. A = 22 J·mol^{-1}·K^{-1} and C = 8 kJ·mol^{-1}). Following the Equation 15, the excess entropy associated to the phase transition at Tc = 348 K is ΔS = 11 J·mol^{-1}·K^{-1}.
Such a very small value agrees with that reported for a similar compound by Boerio-Goates et al.[32]

CONCLUSIONS

The tricritical phase transition between the ferroelastic (monoclinic) and the paraelastic (orthorhombic) phase in ZSM-5 zeolite can be considered in conjunction with the reported occurrence, within orthorhombic ZSM-5 crystals, of a lattice strain revealed as an unusual deformation field distribution observed by coherent X-ray diffraction imaging.[45] In fact, the lattice strain should be absent in the paraelastic phase. However, it has been suggested that the crystal structure of the ferroelastic phase can be maintained on a local scale even in the paraelastic phase.[36] This would lead to the formation of ferroelastic domains whose boundaries would be highly mobile.[36] Upon thermal excitation, the crystal would behave as macroscopically paraelastic and no macroscopic domain switching would occur. Domain structure materials showing a tricritical phase transition, which can be taken as the borderline between a second order and first order transition, generally exhibit less relevant strain fluctuations compared to materials with second order phase transitions.[36] The close interplay between atomistic, micro-structural, and thermodynamic properties in the ZSM-5 zeolite, as we detailed in the present work, allow to set more definite boundaries when modeling, and engineering,[45] the macroscopic strain effects on adsorption and diffusion of guest molecules in this microporous material widely employed in catalysis and water treatment processes.

ACKNOWLEDGEMENTS

This study was carried out within a project founded by the "SoWaZe" PRIN program of the Italian Ministry for University and Research (MIUR). We acknowledge the European Synchrotron Radiation Facility (ESRF, Grenoble) for provision of beamtime to proposal CH-3510 "*In situ XRD study of structural modifications and desorption kinetics of zeolites used for removal of non polar organic compounds from contaminated water*".

REFERENCES

(1) Baerlocher, C.; McCusker, L.B.; Olson, D.H. *Atlas of Zeolite Framework Types*, 6th ed.; Elsevier: Amsterdam, 2007.

(2) Kokotailo, G.T.; Lawton, S.L.; Olson, D.H; Meier, W.M. Structure of Synthetic Zeolite ZSM-5. *Nature* **1978**, *272*, 437–438.

(3) van Koningsveld, H.; Tuinstra, F.; Jansen, J.C.; van Bekkum, H. On the Preparation of a Monoclinic (Nearly) Single Crystal of Zeolite HZSM-5. *Zeolites* **1989**, *9*, 253–256.

(4) van Koningsveld, H.; Jansen, J.C.; van Bekkum, H. The Monoclinic Framework Structure of Zeolite H-ZSM-5. Comparison With the Orthorhombic Framework of as-Synthesized ZSM-5. *Zeolites* **1990**, *10*, 235–242.

(5) Kamiya, N.; Yano, M.; Matsuo, H.; Iwama, W.; Nishi, K.; Yokomori, Y. Simple Method for Preparing Monoclinic Single Crystals of Zeolite ZSM-5 and Analysis of Their Structure. *Z. Kristallogr.* **2010**, *225*, 139–145.

(6) van Koningsveld, H.; Jansen, J.C.; van Bekkum, H. The Orthorhombic/Monoclinic Transition in Single Crystals of Zeolite ZSM-5. *Zeolites* **1987**, *7*, 564–568.

(7) van Koningsveld, H. High-Temperature (350 K) Orthorhombic Framework Structure of Zeolite H-ZSM-5. *Acta Cryst.* **1990**, *B46*, 731–735.

(8) Artioli, G.; Lamberti, C.; Marra, G.L. Neutron Powder Diffraction Study of Orthorhombic and Monoclinic Defective Silicalite. *Acta Cryst*. **2000**, *B56*, 2–10,

(9) Millini, R.; Previde Massara, E.; Perego, G.; Bellussi, G. Framework Composition of Titanium Silicalite-1. *J. Catal.* **1992**, *137*, 497–503.

(10) Lamberti, C.; Bordiga, S.; Zecchina, A.; Carati, A.; Fitch, A.N.; Artioli, G.; Petrini, G.; Salvalaggio, M.; Marra, G.L. Structural Characterization of Ti-Silicalite-1: A Synchrotron Radiation X-Ray Powder Diffraction Study. *J. Catal.* **1999**, *183*, 222–231.

(11) Leardini, L.; Martucci, A.; Cruciani G. The Unusual Thermal Behaviour of Boron-ZSM-5 Probed by "*In Situ*" Time-Resolved Synchrotron Powder Diffraction. *Micropor. Mesopor. Mat.* **2013**, *173*, 6–14.

(12) Marra, G.L.; Tozzola, G.; Leofanti, G.; Padovan, M.; Petrini, G.; Genoni, F.; Venturelli, B.; Zecchina, A.; Bordiga, S.; Ricchiardi, G. Orthorhombic and Monoclinic Silicalites: Structure, Morphology, Vibrational Properties and Crystal Defects. *Stud. Surf. Sci. Catal.* **1994**, *84*, 559–566.

(13) Mentzen, B.F.; Letoffe, J.-M.; Claudy, P. Enthalpy Change and Temperature of the Reversible Monoclinic-Orthorhombic Phase Transition in MFI Type Zeolitic Materials. *Thermochim. Acta* **1996**, *288*, 1–7.

(14) Wu, E.L.; Lawton, S.L.; Olson, D.H.; Rohrman, A.C.; Kokotailo, G.T. ZSM-5-Type Materials. Factors Affecting Crystal Symmetry. *J. Phys. Chem.* **1979**, *83*, 2777–2781.

(15) Hay, D.G.; Jaeger, H.; West, G.W. Examination of the Monoclinic/Orthorhombic Transition in Silicalite Using XRD and Silicon NMR. *J. Phys. Chem.* **1985**, *89*, 1070–1072.

(16) Mentzen, B.F.; Sacerdote-Peronnet, M. Flexibility of the Framework Structure in Highly Crystalline Silicalite During the Reversible Monoclinic/Orthorhombic Solid State Polymorphic Phase Transition. *Mater. Res. Bull.* **1993**, *28*, 1017–1024.

(17) Endoh, A. Calorimetric Study of the Monoclinic-Orthorhombic Phase Transition in Highly Siliceous Zeolite ZSM-5. *Zeolites* **1988**, *8*, 250–251.

(18) Fujiyama, S.; Kamiya, N.; Nishi, K.; Yokomori, Y. Location of CO_2 on Silicalite-1 Zeolite Using a Single-Crystal X-Ray Method. *Z. Kristallogr.* **2013**, *228*, 180–186.

(19) Martucci, A.; Pasti, L.; Nassi, M.; Alberti, A.; Arletti, R.; Bagatin, R.; Vignola, R.; Sticca, R. Adsorption Mechanism of 1,2-Dichloroethane into an Organophilic Zeolite Mordenite: A Combined Diffractometric and Gas Chromatographic Study. *Micropor. Mesopor. Mat.* **2012**, *151*, 358–367.

(20) Pasti, L.; Martucci, A.; Nassi, M.; Cavazzini, A.; Alberti, A.; Bagatin, R. The Role of Water in DCE Adsorption from Aqueous Solutions onto Hydrophobic Zeolites. *Micropor. Mesopor Mat.* **2012**, *160*, 182–193.

(21) van Koningsveld, H.; Jansen, J.C. Preparation and Structure of Crystals of Zeolite H-ZSM-5 Loaded With *p*-Nitroaniline. *Micropor. Mat.* **1996**, *6*, 159–167.
(22) Nishi, K.; Hidaka, A.; Yokomori, Y. Structure of Toluene6.4-ZSM-5 and the Toluene Disproportionation Reaction on ZSM-5. *Acta Cryst.* **2005**, *B61*, 160–163.
(23) van Koningsveld, H.; Tuinstra, F. The Location of *p*-Xylene in a Single Crystal of Zeolite H-ZSM-5 with a New, Sorbate-Induced, Orthorhombic Framework Symmetry. *Acta Cryst.* **1989**, *B45*, 423–431.
(24) van Koningsveld, H.; Jansen, J.C.; de Man, A.J.M. Single-Crystal Structure Analysis and Energy Minimizations of a MFI-Type Zeolite at Low *p*-Dichlorobenzene Sorbate Loading. *Acta Cryst.* **1996**, *B52*, 131–139.
(25) van Koningsveld, H.; Jansen, J.C.; van Bekkum, H. The Location of *p*-Dichlorobenzene in a Single Crystal of Zeolite H-ZSM-5 at High Sorbate Loading. *Acta Cryst.* **1996**, *B52*, 140–144.
(26) van Koningsveld, H.; Koegler, J.H. Preparation and Structure of Crystals of Zeolite H-ZSM-5 Loaded With *p*-Nitroaniline. *Micropor. Mat.* **1997**, *9*, 71–81.
(27) Kamiya, N.; Oshiro, T.; Tan, S.; Nishi, K.; Yokomori, Y. Adsorption Process of Phenol on Silicalite-1 and Crystal Structure of Phenol8.0–Silicalite-1 Using a Single Crystal X-Ray Diffraction Method. *Micropor. Mesopor. Mat.* **2013**, *169*, 168–175.
(28) Nishi, K.; Yokomori, Y. Determining the Structure of a Benzene7.2-Silicalite-1 Zeolite Using a Single-Crystal X-Ray Method. *Acta Cryst.* **2011**, *B67*, 508–515.
(29) Fujiyama, S.; Kamiya, N.; Nishi, K.; Yokomori, Y. Reanalysis of CO_2-Silicalite-1 Structure as Monoclinic Twinning. *Z. Kristallogr.* **2014**, *229*, 303–309.
(30) Fujiyama,S.; Seino, S.; Kamiya, N.; Nishi, K.; Yozab, K.; Yokomoria, Y. Adsorption Structures of Non-Aromatic Hydrocarbons on Silicalite-1 Using the Single-Crystal X-Ray Diffraction Method. *Phys. Chem. Chem. Phys.* **2014**, *16*, 15839–15845.
(31) Kamiya, N.; Iwama, W.; Kudo, T.; Nasuno, T.; Fujiyama, S.; Nishi, K.; Yokomori, Y. Determining the Structure of a Benzene7.2-Silicalite-1 Zeolite Using a Single-Crystal X-Ray Method. *Acta Cryst.* **2011**, *B67*, 508–515.
(32) Boerio-Goates, J.; Stevens, R.; Hom, B.; Piccione, P.; Davis, M.; Navrotsky, A. Heat Capacities, Third-Law Entropies and Thermodynamic Functions of SiO_2 Molecular Sieves from T = 0 K to 400 K. *J. Chem. Thermodyn.* **2002**, *34*, 205–227.
(33) Toby, H. *EXPGUI*, a Graphical User Interface for *GSAS*. *J. Appl. Crystrallogr.* **2001**, *34*, 210–213.
(34) Larson, A.; Von Dreele, R. *General structure analysis system (GSAS)*; Los Alamos National Laboratory Report LAUR: 86-748, 2004.
(35) van Koningsveld, H.; van Bekkum, H.; Jansen, J.C. On the Location and Disorder of the Tetrapropylammonium (TPA) Ion in Zeolite ZSM-5 with Improved Framework Accuracy. *Acta Cryst.* **1987**, *B43*, 127–132.
(36) Salje, E. *Phase transition in ferroelastic and co-elastic crystals*; Cambridge University Press: Cambridge, 1990.
(37) Carpenter, M.; Salje, E.; Graeme-Barber, A. Spontaneous Strain as a Determinant of Thermodynamic Properties for Phase Transitions in Minerals. *Eur. J. Mineral.* **1998**, *10*, 621–691.
(38) Salje, E.; Wruck, B.; Thomas, H. Order-Parameter Saturation and Low-Temperature Extension of Landau Theory. *Z. Phys. B Con. Mat.* **1991**, *82*, 399–404.
(39) Angel, R.J.; Gonzalez-Platas, J.; Alvaro, M. EosFit7c and a Fortran Module (Library) for Equation of State Calculations. *Z. Kristallogr.* **2014**, *229*, 405–419.
(40) Fei, Y. *Thermal expansion*; in T. Ahrens, ed. "Mineral physics & crystallography: A handbook physical constants", AGU: Washington DC, 1995.
(41) Bhange, D.; Ramaswamy, V. Negative Thermal Expansion in Silicalite-1 and Zirconium Silicalite-1 Having MFI Structure. *Mater. Res. Bull.* **2006**, *41*, 1392–1402.
(42) Aizu, K. Determination of the State Parameters and Formulation of Spontaneous Strain for Ferroelastics. *J. Phys. Soc. Jpn.* **1970**, *28*, 706–716.

(43) Putnis, A. *Introduction to mineral sciences*; Cambridge University Press: Cambridge, 1992.
(44) Cámara, F.; Nestola, F.; Angel, R.; Ohashi, H. Spontaneous Strain Variations Through the Low-Temperature Displacive Phase Transition of $LiGaSi_2O_6$ Clinopyroxene. *Eur. J. Mineral.* **2009**, *21*, 599–614.
(45) Cha, W.; Jeong, N.C.; Song, S.; Park, H.; Thanh Pham, T.C.; Harder, R.; Lim, B.; Xiong, G.; Ahn, D.; McNulty, I. et al. Core-Shell Strain Structure of Zeolite Microcrystals. *Nat. Mater.* **2013**, *12*, 729–734.